New lifetime measurement for the 2_1^+ level in ^{112}Sn by the Doppler-shift attenuation method

A. Kundu,[1,*] Md. S. R. Laskar,[1] R. Palit,[1,†] R. Raut,[2] S. Santra,[3,8] N. Shimizu,[4] T. Togashi,[4] E. Ideguchi,[5] H. Pai,[6] S. Ali,[6] F. S. Babra,[1] R. Banik,[7,8,‡] Soumik Bhattacharya,[7] S. Biswas,[1] Biswajit Das,[1] P. Dey,[1] R. Donthi,[1] A. Goswami,[6,§] S. Jadhav,[1] G. Mukherjee,[7] B. S. Naidu,[1] S. Rajbanshi,[9] L. P. Singh,[1] H. P. Sharma,[10] S. S. Tiwary,[10] and A. T. Vazhappilly[1]

[1]*Department of Nuclear and Atomic Physics, Tata Institute of Fundamental Research, Mumbai 400005, India*
[2]*UGC-DAE Consortium for Scientific Research, Kolkata Centre, Kolkata 700098, India*
[3]*Nuclear Physics Division, Bhabha Atomic Research Centre, Mumbai 400085, India*
[4]*Center for Nuclear Study, The University of Tokyo, Hongo, Bunkyo-ku, Tokyo 113-0033, Japan*
[5]*Research Center for Nuclear Physics (RCNP), Osaka University, Ibaraki, Osaka 567-0047, Japan*
[6]*Nuclear Physics Division, Saha Institute of Nuclear Physics, Kolkata 700064, India*
[7]*Variable Energy Cyclotron Centre, 1/AF Bidhan Nagar, Kolkata 700064, India*
[8]*Homi Bhabha National Institute, Anushaktinagar, Mumbai 400094, India*
[9]*Department of Physics, Presidency University, Kolkata 700073, India*
[10]*Department of Physics, Institute of Science, Banaras Hindu University, Varanasi 221005, India*

(Received 20 November 2020; revised 3 February 2021; accepted 25 February 2021; published 22 March 2021)

Levels in the ^{112}Sn nucleus have been excited by inelastic scattering with ^{35}Cl projectile at $E_{\rm lab} = 195$ MeV. The Doppler affected γ-ray peak arising from the decay of the 2_1^+ level has been analyzed, using updated methodologies, to extract the level lifetime and corresponding electric quadrupole ($E2$) transition probability, $B(E2; 0^+_{\rm g.s.} \rightarrow 2_1^+)$. The present result is discrepant with respect to the results reported from existing lifetime measurements, but in compliance with independent systematic measurements of the low-lying $E2$ transition strengths in the stable even-mass Sn isotopes, by pure Coulomb excitation as well as heavy-ion induced inelastic collisions. The transition probability also confirms an enhancement in collectivity for the 2_1^+ level, and is found to be in good agreement with generalized seniority model (GSM) as well as state-of-the-art Monte Carlo shell model (MCSM) calculations. Within the realm of the MCSM scheme, the enhancement is understood in terms of oblate deformations for both the $0^+_{\rm g.s.}$ and 2_1^+ states in ^{112}Sn arising due to strong proton-core excitations and enhanced proton-neutron interactions. In addition, limits for the lifetime of the 3_1^- level and the $E1$ transition probability, $B(E1; 3_1^- \rightarrow 2_1^+)$, have been obtained.

DOI: 10.1103/PhysRevC.103.034315

I. INTRODUCTION

The evolution of transition probabilities, a signature of nuclear collectivity (or deformation), to the low-lying excited states in the series of Sn isotopes, has been under discussion for several years and still attracts interest with regard to its understanding in various models. In this context, the 2_1^+ state in the stable even-mass $^{112-124}$Sn region has been extensively probed by means of Coulomb excitation [1–5], nuclear resonance fluorescence [6], and inelastic scattering of electrons [7], protons [8,9], α particles [10], and heavy ions [11–13]. These methods are fairly consistent with one another, with the transition probabilities often measured with small uncertainties, and also consolidated into the adopted $B(E2; 0^+_{\rm g.s.} \rightarrow 2_1^+)$ values by Raman *et al.* [14]. Conventionally, collectivity along an isotopic chain is expected to be at its highest when the number of nucleons outside closed shells is largest, i.e., around midshell, with subsequent decrease as the neutron number varies on either side. Several theoretical frameworks have similarly predicted a parabolic trend, peaked at ^{116}Sn, in the development of the $B(E2; 0^+_{\rm g.s.} \rightarrow 2_1^+)$ values along the $^{102-130}$Sn chain, based on exact seniority model calculations [15] as well as large-scale shell model calculations considering (i) an inert ^{100}Sn core with only valence neutrons or (ii) an inert ^{90}Zr core involving proton excitations along with valence neutrons [16]. From the existing measurements, such an evolution has been observed in the $B(E2; 0^+_{\rm g.s.} \rightarrow 2_1^+)$ values for the isotopes with mass $A \geqslant 116$ by Coulomb-excitation measurements extending up to the neutron-rich $^{126-130}$Sn isotopes [17]. However, for $A < 116$, the measured $B(E2; 0^+_{\rm g.s.} \rightarrow 2_1^+)$ values are seen to increase from ^{116}Sn up to ^{112}Sn and stay nearly similar up to ^{106}Sn, thereafter decreasing towards ^{104}Sn [18–21]. Another set of calculations employing the relativistic quasiparticle random phase approximation (RQRPA) [22] have been fairly successful in explaining the larger values observed for the neutron-deficient unstable region of the series; however, they predict values suppressed by 30–40% for the stable $^{112-124}$Sn

*ananyak.delhi@gmail.com
†palit@tifr.res.in
‡Present address: Institute of Engineering and Management, Saltlake Sector V, Kolkata 700091, India.
§Deceased.

region, compared to existing experimental results. Owing to the limitations of the aforementioned calculations, further attempts were made by employing the (i) generalized-seniority model (GSM) [15,23], and (ii) state-of-the-art Monte Carlo shell model (MCSM) [24–26] formalisms. The former emphasizes the different rates of filling of orbits along the Sn chain, and divides the neutron valence space into two parts prior to and post the midshell, giving rise to two asymmetric parabolas with a valley at ^{116}Sn. On the other hand, the latter is a novel attempt to present a unified picture across the full Sn series by employing a large model space including single-particle orbits for the protons and neutrons, wherein the protons in the $1g_{9/2}$ orbital are taken to be fully activated. The robust MCSM calculations for the $^{100-138}$Sn chain [26] are found to successfully concur with the evolution of the measured $B(E2; 0^+_{\rm g.s.} \rightarrow 2^+_1)$ values across the Sn series, and are in reasonable agreement with the GSM calculations for the $^{104-130}$Sn region reported in Ref. [23]. In a complementary approach, direct measurements of the level lifetimes for the collective low-spin states in Sn isotopes were recently attempted using the Doppler-shift attenuation method (DSAM) [27]. In the measurements of the 2^+_1 level lifetimes along the $^{112-124}$Sn series reported by Jungclaus *et al.* [28,29], the corresponding $B(E2; 0^+_{\rm g.s.} \rightarrow 2^+_1)$ values are seen to exhibit a systematic trend of reduced collectivity, with a valley at ^{116}Sn, as also predicted by the MCSM and GSM approaches. However, there is an overall departure of the absolute values from the calculations. The measurements were performed in inverse kinematics at high beam energies, thereby populating several excited states above the 2^+_1 state. The corresponding feedings from the 4^+_1 and 3^-_1 levels were reported to be dominant. While the 4^+_1 state is known to be substantially long-lived to show any considerable Doppler shifted (feeding) fraction in the $2^+_1 \rightarrow 0^+_{\rm g.s.}$ transition, the 3^-_1 state is short-lived and has been reported to constitute about 15–30% of the $2^+_1 \rightarrow 0^+_{\rm g.s.}$ intensity [28]. A comparison of the 2^+_1 lifetimes measured by Jungclaus *et al.* with those inferred from the adopted $B(E2; 0^+_{\rm g.s.} \rightarrow 2^+_1)$ values [14] indicate a discrepancy, with the former being significantly longer. Simultaneous estimates of the lifetimes of the feeder states are therefore crucial for determining the lifetime of the 2^+_1 state. For the low-lying states in ^{112,114}Sn, Spieker *et al.* [30] very recently used the $(p, p'\gamma)$ reaction to probe the lifetimes using DSAM, without feeding contributions, by employing particle(proton)-γ coincidence. An Sn-Au alloy was bombarded in the measurement, where the target and stopper material were not completely separated. Previous measurements on proton inelastic scattering from the stable Sn isotopes [8,9] have observed transitions to the 2^+_1 and 3^-_1 levels to be dominant over other neighboring states. However, in the particle-energy spectrum reported by Spieker *et al.* for the ^{112}Sn(p, p') reaction, beyond the excitation corresponding to the 2^+_1 state, well-resolved peaks for higher excited states are not seen. In particular, the 3^-_1 state is not observed to be strongly populated, with possible ambiguity in identifying the exact centroid energy. Interestingly, the 2^+_1 and 3^-_1 lifetimes from this work are reported to be longer and shorter, respectively, than those measured by Jungclaus *et al.* The results reported by Spieker *et al.* as well as Jungclaus *et al.* also contradict the lifetimes deduced using DSAM from a set of extensive measurements of the low-lying structure in ^{112}Sn by the ^{112}Sn$(n, n'\gamma)$ reaction [31–33].

In order to address the disagreements across different categories of experiments and to regard an old question from a fresh perspective, new measurements of lifetimes for the low-lying levels in the stable Sn isotopes are warranted, to facilitate concluding on the transition probabilities determined therefrom. Such an exercise was recently attempted by means of heavy-ion inelastic scattering for the 2^+_1 lifetime in the ^{120}Sn isotope [34], and the corresponding result leads to an improved estimate. The measurement reported in Ref. [34] was performed at a bombarding energy below the Coulomb barrier and, as a result, additional states in ^{120}Sn were not populated significantly, leading to inconsequential feeding to the 2^+_1 state. The present work takes another step in this direction and reports a fresh measurement of lifetime of the 2^+_1 ($E_{\rm x} = 1257$ keV) level in the ^{112}Sn isotope, populated by means of heavy-ion inelastic collision at a high bombarding energy.

II. MEASUREMENT

Multiple excited states of ^{112}Sn nucleus were populated using the ^{112}Sn(^{35}Cl, ^{35}Cl$'$) ^{112}Sn* heavy-ion inelastic scattering process at $E_{\rm lab} = 195$ MeV. The ^{35}Cl beam was provided by the BARC-TIFR Pelletron LINAC Facility, Mumbai. Beam energy above the Coulomb barrier ($V_{\rm B} \approx 136$ MeV) facilitated substantial population of the 2^+_1 level at an excitation energy of 1257 keV. In addition, the 3^-_1 level at 2354 keV, which decays to the 2^+_1 level, was also found to be populated, thus enabling a coincidence analysis. The excitation is governed by well defined two-body kinematics and energetics. The target comprised an enriched (99.6%) ^{112}Sn foil of thickness $\approx$2.4 mg/cm^2, with a ^{208}Pb backing of thickness $\approx$8.8 mg/cm^2 [35]. Emitted γ rays from the recoiling ^{112}Sn nuclei were detected using the Indian National Gamma Array (INGA) [36], then consisting of eleven Compton-suppressed high-purity germanium (HPGe) clover detectors, mounted at a distance of 25 cm from the target center. The clovers were distributed at angles $\theta = 90^{\rm o}$ (three at $\phi = 60^{\rm o}$, $120^{\rm o}$, $300^{\rm o}$), $\theta = 115^{\rm o}$ (two at $\phi = 90^{\rm o}$, $330^{\rm o}$), $\theta = 140^{\rm o}$ (three at $\phi = 0^{\rm o}$, $120^{\rm o}$, $240^{\rm o}$) and $\theta = 157^{\rm o}$ (three at $\phi = 60^{\rm o}$, $180^{\rm o}$, $300^{\rm o}$), with respect to the beam direction. Levels with spins up to 8^+ and 9^- were populated in ^{112}Sn in the present measurement, as also previously observed in experiments involving neutron scattering [31] and/or fusion-evaporation [37]. A typical spectrum gated with the $2^+_1 \rightarrow 0^+_{\rm g.s.}$ transition is shown in Fig. 1, displaying some of the dominant (parallel) decay paths. Owing to the extended angular range of γ-decay positions as permitted by inelastic scattering, each HPGe detector recorded an inclusive decay spectrum for scattering at all possible recoil directions. The detectors were calibrated in energy and efficiency using standard ^{133}Ba - ^{152}Eu sources. An energy resolution of $\approx$2.6 keV was obtained at an energy of 1408 keV. Time stamped list mode spectroscopic data were acquired using a digitizer-based data acquisition system. The acquired decay events were sorted into E_γ-E_γ correlation matrices using the MARCOS [38] code. These matrices were

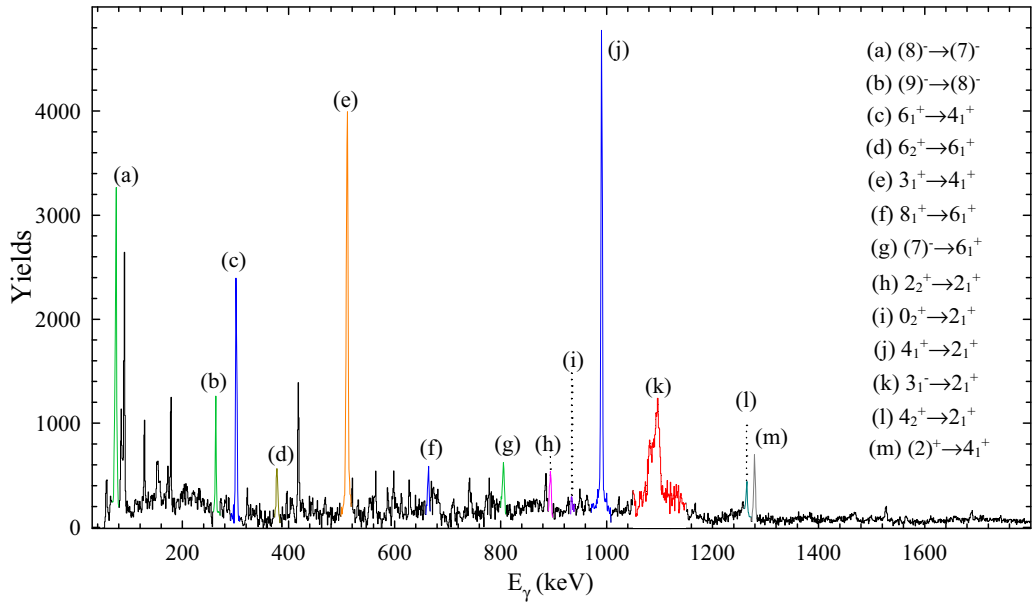

FIG. 1. Experimental γ-ray spectrum showing transitions in ^{112}Sn in coincidence with the $2_1^+ \rightarrow 0_{g.s.}^+$ transition. Various γ rays of ^{112}Sn, namely, (a) 76 keV, (b) 263 keV, (c) 302 keV, (d) 378 keV, (e) 510 keV (509 keV as seen in Ref. [31], with some admixture from the 511 keV annihilation γ ray), (f) 664 keV, (g) 805 keV, (h) 894 keV, (i) 934 keV, (j) 991 keV, (k) 1097 keV, (l) 1264 keV, and (m) 1278 keV, which were also observed in previous measurements on neutron scattering [31] and/or fusion-evaporation [37], have been marked in the spectrum. The 2_1^+ state is fed through such parallel decay paths, marked with different colors. The $3_1^- \rightarrow 2_1^+$ transition is seen with a Doppler broadened line shape, unlike the other stopped peaks.

angle-dependent asymmetric ones for lifetime analysis and had detectors at a given angle θ on the X axis (summed over the different ϕ angles), with detectors at all the other angles on the Y axis. The Doppler-affected shapes on the transition peaks at different angles, as observed in the spectra with a gate set on coincident transitions (following the deexcitation of the 2_1^+ and 3_1^- states), were analyzed to extract level lifetimes of interest, as elaborated in the subsequent text.

III. LIFETIME ANALYSIS AND RESULTS

The γ rays are emitted in-flight, with the recoiling ^{112}Sn nuclei in relative motion with respect to the detectors in the array, and thus exhibit Doppler effect as expected. Analysis for determining the lifetime of the 2_1^+ in ^{112}Sn was carried out using the developments by Das *et al.* [39] in conjunction with the LINESHAPE [40] package. The analysis was based on the coincidence spectra of the $3_1^- \rightarrow 2_1^+$ (Fig. 2) and the $2_1^+ \rightarrow 0_{g.s.}^+$ (Fig. 3) transitions, in cascade. As such, the population and the kinematics of only the 3_1^- state are of pertinence in this exercise; the population of the 2_1^+ level, as is manifested in the coincidence data, is that which is fed by the 3_1^- state above. Such an analysis of Doppler shapes following γ-ray measurements in coincidence mode, without having to compromise on the counting statistics for $E_{lab} \gg V_B$, bears the advantage of narrowing down to this specific decay path. The 3_1^- state can have different possible decay modes [41] such as (i) an $E1$ ($3_1^- \rightarrow 2_1^+$) transition, $E_\gamma = 1097$ keV, and (ii) an $E1$ ($3_1^- \rightarrow 2_2^+$) transition, $E_\gamma = 203$ keV. Additionally, as observed for some of the neighboring stable Sn isotopes, namely ^{116,118,122}Sn, a weak $E3$ ($3_1^- \rightarrow 0_{g.s.}^+$) transition may also be probable. However, the latter two are not observed in the present measurement and the decay of the 3_1^- state

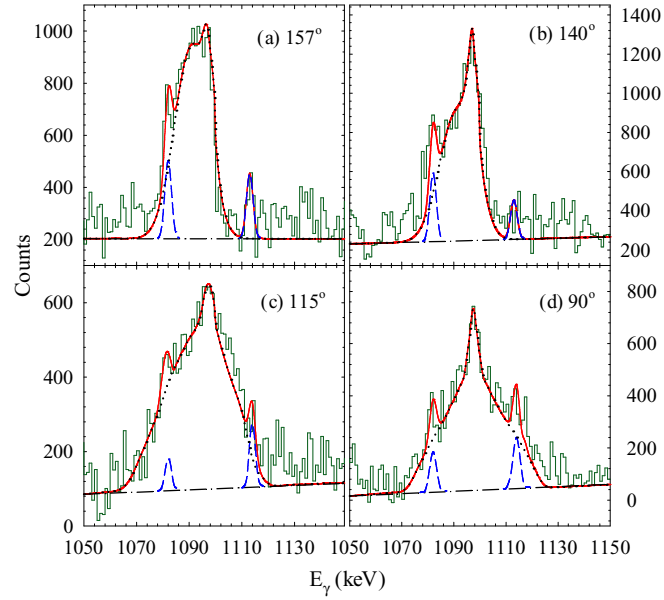

FIG. 2. Experimental Doppler broadened γ-ray peak of the 1097-keV ($3_1^- \rightarrow 2_1^+$) transition in ^{112}Sn spectra gated with the $2_1^+ \rightarrow 0_{g.s.}^+$ transition (gated from below), and corresponding fits obtained using the LINESHAPE code. The dashed lines represent deconvoluted fit of the additional stopped peaks in the fitting range (please see text for details). The dotted lines represent the exclusive transition line shape, while the solid lines show the total fit.

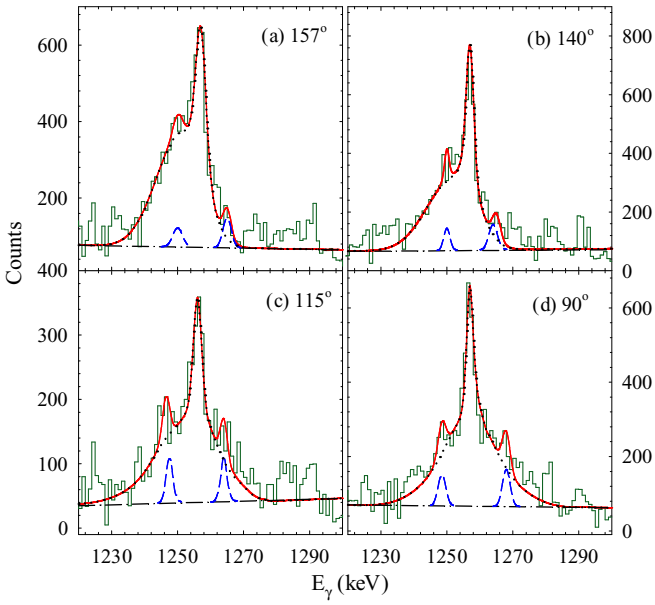

FIG. 3. Experimental Doppler broadened γ-ray peak of the 1257-keV ($2_1^+ \rightarrow 0_{\text{g.s.}}^+$) transition in ^{112}Sn spectra gated with the $3_1^- \rightarrow 2_1^+$ transition (gated from above), and corresponding fits obtained using the LINESHAPE code. The dashed lines represent deconvoluted fit of the additional stopped peaks in the fitting range (please see text for details). The dotted lines represent the exclusive transition line shape, while the solid lines show the total fit.

predominantly occurs by a fast $E1$ transition of $E_\gamma = 1097$ keV to the 2_1^+ state, which subsequently decays to the $0_{\text{g.s.}}^+$ state by an $E2$ transition of energy $E_\gamma = 1257$ keV. These states are known to have nearly 100% γ branching.

The analysis for the level lifetimes commences with the simulation of the trajectories of ^{112}Sn nuclei scattered to their 3_1^- state and traversing the target and the backing media. The considerable thickness of the ^{112}Sn target incurs loss of beam energy along its depth (a degradation of $\approx$17 MeV) and warrants incorporation of additional effects in the stopping simulations. These are (i) the evolving inelastic scattering cross section to the 3_1^- state, with changing beam energy, and (ii) the corresponding energy-angle distributions of the recoiling nuclei. The cross sections for excitation to the 3_1^- state at different beam energies along the target depth were calculated in the framework of a coupled reaction channels (CRC) model using the FRESCO [42] code. The CRC calculationwere performed by coupling the major inelastic scattering channels to the entrance channel, which include (i) the low-lying 2_1^+ and 3_1^- states of ^{112}Sn at $E_x = 1257$ keV and 2354 keV, respectively, treated as collective vibrational one-phonon quadrupole and octupole states with $B(E2; 0_{\text{g.s.}}^+ \rightarrow 2_1^+) = 0.250\ e^2\text{b}^2$ [5] and $B(E3; 0_{\text{g.s.}}^+ \rightarrow 3_1^-) = 0.087\ e^2\text{b}^3$ [3], and (ii) the 4_1^+ state of ^{112}Sn at $E_x = 2247$ keV, treated as a collective vibrational double-quadrupole-phonon state with $B(E2; 4_1^+ \rightarrow 2_1^+) = 0.018\ e^2\text{b}^2$ [3]. For completeness, a few one-nucleon transfer channels are also coupled with unit spectroscopic factors. The projectile-target interaction is governed by the Coulomb potential and an optical nuclear potential of Woods Saxon form, with a short-ranged imaginary part to account for the fusion process. The potential parameters were suitably adjusted to closely reproduce the available experimental cross sections [43] for the complete fusion of ^{35}Cl with ^{112}Sn at different energies.

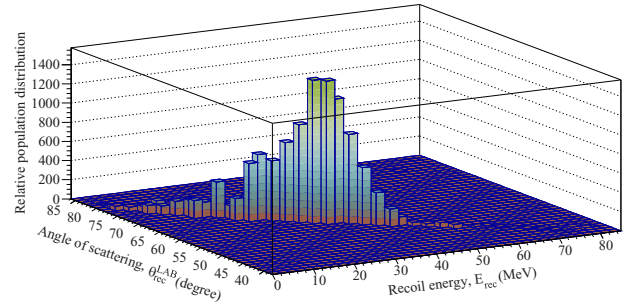

FIG. 4. Typical calculated relative population distribution of the scattered ^{112}Sn recoils in their 3_1^- excited state as a function of laboratory scattering angle $\theta_{\text{rec}}^{\text{LAB}}$ and kinetic energy E_{rec}, in the $^{35}\text{Cl} + ^{112}\text{Sn}$ system at $E_{\text{lab}} = 195$ MeV.

Across the full target depth, the production of the recoiling nuclei was estimated to be significant, with the estimated cross section at the bombarding energy of 178 MeV decreasing by only 10% compared to the cross section at the beam energy of 195 MeV. The thickness of the target was accordingly binned into four sections of decreasing beam energy, each characterized by individual yields of the ^{112}Sn recoils scattered in the 3_1^- state and the energy-angle distribution of the same. The energy-angle distribution of the recoils, collated from those corresponding to individual beam energies, is illustrated in Fig. 4. The other cardinal component of the stopping simulations is the stopping power of the target and the backing media for the recoils. The stopping power is also accepted as one of the principal sources of uncertainties in the lifetime analysis. Earlier developments in the stopping power modeling by Lindhard *et al.* [44], Ziegler [45], as well as Northcliffe and Schilling [46] are known to be characterized by uncertainties of $\approx$10–15%, particularly at low kinetic energies [47]. These models have been adopted in the existing lifetime analyses reported for the Sn isotopes [28–32]. The present analysis is based on the use of experimentally-benchmarked stopping powers calculated by the SRIM code that are characterized by a modest uncertainty $\approx$ 5% [48], representing a significant improvement over the previous modelings. These stopping powers are used to simulate the ion transport in the TRIM software and the results go as inputs to the developments by Das *et al.* [39] to calculate the trajectories of ^{112}Sn in the target and the backing media, in time steps of 0.002 ps. The origins of the trajectories were distributed across the thickness of the target, binned, as mentioned earlier, into four segments. These trajectories are used by the HISTAVER program of the LINESHAPE [40] package to calculate the velocity profiles of the recoils, as viewed by the γ-ray detectors. These profiles then go, as inputs, into the LINESHAPE code that uses them, along with the level scheme information (γ-ray energies, feeding intensities, branching ratios, etc.), to calculate the Doppler shapes on the γ-ray transitions (peaks) of interest.

TABLE I. Lifetime $\tau_{3_1^-}$ and transition probability $B(E1; 3_1^- \rightarrow 2_1^+)$ for the 3_1^- state in ^{112}Sn, compared with existing estimates.

[a]$\tau_{3_1^-}$ [a] (ps)	[b]$\tau_{3_1^-}$ [b] (ps)	[c]$\tau_{3_1^-}$ [c] (ps)	[d]$\tau_{3_1^-}$ [d] (ps)	[a]$B(E1)$[a] (e^2b)
$\leqslant 0.537$	$0.51^{+0.20}_{-0.12}$	0.280(20)	0.31(2)	$\geqslant 8.87 \times 10^{-6}$

[a]Present measurement.
[b]^{112}Sn$(n, n'\gamma)$ [31]
[c]^{112}Sn$(p, p'\gamma)$ Spieker *et al.* [30]
[d]Jungclaus *et al.* [28]

The calculated shapes are least square fitted to the experimental spectra in order to extract the lifetime results. The fitting parameters include the lifetime/transition quadrupole moment, the side feeding (if any) time and the spectral parameters such as the background, the peak heights, etc. The procedure of fitting the Doppler shapes, as applied in the present analysis, is detailed in Refs. [34,49]. In the current analysis, spectra at four different angles were fitted simultaneously as per the standard procedure. This facilitates constraining the multiple parameters associated with the minimization exercise.

In the first part of the analysis, the Doppler shapes on the $3_1^- \rightarrow 2_1^+$ transition peak were analyzed in the spectra with a gate on the $2_1^+ \rightarrow 0_{\text{g.s.}}^+$ transition. The contribution of the feedings in the population of the 3_1^- state assumes pertinence therein. In this work, the possible feedings are seen to be from the levels (transitions) at E_x $(E_\gamma) = 2966$ (612), 3133 (779), and 3248 (894) keV, with the 779 keV transition being the most dominant. However, each individual feeder state is found to be only tenuously populated, as observed from the experimental spectra, and also when included as an additional channel (with different sets of relevant structural parameters) in the theoretical model of the CRC calculations, thereby restricting a top-gated analysis. Consequently, the effective feeding was modelled in the LINESHAPE code by a single level populating the 3_1^- state, with a feeding intensity amounting to $\approx$11%, obtained from the difference in the intensities of the $3_1^- \rightarrow 2_1^+$ transition peak and the summed intensities of the peaks corresponding to the feeding transitions originating from the aforementioned levels, in the spectrum with gate on the $2_1^+ \rightarrow 0_{\text{g.s.}}^+$ transition. From the line shape fit for the $3_1^- \rightarrow 2_1^+$ transition in the present analysis, an effective lifetime value of $0.489^{+0.048}_{-0.056}$ ps is obtained. The quoted statistical uncertainties were derived from χ^2 analysis of the fitted lifetime values. This analysis defines an upper limit for the lifetime of the 3_1^- state, $\tau_{3_1^-} \leqslant 0.537$ ps. The result does not include the systematic effect of the uncertainties on the stopping powers. However, given that these were from the SRIM code, fairly lower errors are expected than the earlier models used in conventional analyses. This lifetime, when compared with those from the existing measurements, is found to be longer than the values arrived at by Jungclaus *et al.* [28] and Spieker *et al.* [30], but in good agreement with that obtained in the ^{112}Sn$(n, n'\gamma)$ experiment (see Table I). Though the latter employed several incident neutron energies to minimize feeding effects, the results are plagued by larger uncertainties. Considering a 100% $E1$ $(3_1^- \rightarrow 2_1^+)$ branching for the 3_1^- state [41], a lower limit for the $E1$ transition probability, $B(E1; 3_1^- \rightarrow 2_1^+)$, was deduced. This value, also reported in Table I, is found to be similar in order of magnitude to the $B(E1; 3_1^- \rightarrow 2_1^+)$ value obtained for ^{116}Sn $(14 \pm 3 \times 10^{-6}\ e^2\text{b})$ from a direct measurement of the $E1$ branching fraction of $\approx 99.8\%$ [3].

In the second part of the analysis, lifetime of the 2_1^+ level was extracted by fitting the Doppler shapes on the $2_1^+ \rightarrow 0_{\text{g.s.}}^+$ transition peak in the spectra with gate on the $3_1^- \rightarrow 2_1^+$ transition above, including the Doppler-shifted as well as unshifted components. Here, the lifetime of the 3_1^- state was held fixed at the effective value extracted from the fit to the $3_1^- \rightarrow 2_1^+$ transition peak described in the preceding part of the analysis. The analysis with a gate set on the transition above the level of interest eliminates the side feeding contribution to the latter and the resulting lifetime is a definite one without any dependence on the side feeding parameter. The lifetime value of the 2_1^+ state, obtained thereby, is $\tau_{2_1^+} = 0.566^{+0.029}_{-0.038}$ ps. This is shorter than the result reported by Jungclaus *et al.* and Spieker *et al.* (see Table II). The ^{112}Sn$(n, n'\gamma)$ measurement initially reported a lifetime of $0.750^{+0.125}_{-0.090}$ ps for this level [32], which was later revised to a value of $0.535^{+0.100}_{-0.080}$ ps [33]. Figure 2 illustrates the fits for the 1097 keV γ-ray peak, while Fig. 3 illustrates the fits for the 1257 keV γ-ray peak. The origin of the additional (contaminant) peaks observed along with those from ^{112}Sn, as seen in Figs. 2 and 3, was ascertained from an analysis of the γ-γ coincidence data and could be ascribed to the deexciting residues produced in the (i) ^{112}Sn(^{35}Cl, $xnypz\alpha$) fusion-evaporation reaction, as well as (ii) different multinucleon transfer reactions. For the fusion-evaporation channels, the identified products include ^{132,137,140}Nd, ^{132}Pr, ^{141}Pm, etc., as also predicted by statistical model calculations with the PACE [50] code. The transfer reactions populate residues such as ^{105}In, ^{109,111,113}Sn, ^{113}Sb, etc. The contaminant peaks riding on the shapes of the transitions of interest are not expected to be Doppler affected, as they originate from known long-lived states in such residues.

Given the accuracy of the methodology adopted in the present work, with lower uncertainty on the stopping power, combined with improved statistics, the present result is being proposed as an improved lifetime estimate for the 2_1^+ level in ^{112}Sn by the DSAM method. The result, compared with existing measurements, is presented in Table II. From the measured lifetime $\tau_{2_1^+}$, the transition probability for the $2_1^+ \rightarrow 0_{\text{g.s.}}^+$ decay was deduced. As illustrated in Fig. 5, it is noteworthy that the corresponding excitation probability, $B(E2; 0_{\text{g.s.}}^+ \rightarrow 2_1^+) = 5 \times B(E2; 2_1^+ \rightarrow 0_{\text{g.s.}}^+)$, supports an argument of enhanced collectivity, and is in good agreement with the results from some recent Coulomb excitation experiments [4,5], as well as measurements involving n [33], α [10], and heavy-ion scattering [11,13]. Reasonable agreement is also seen with the GSM calculation, represented by the dashed line, which considers a ^{100}Sn core and $1g_{7/2} \otimes 2d_{5/2} \otimes 2d_{3/2} \otimes 3s_{1/2}$ valence space for the series prior to the midshell [23]. The experimental result is also well corroborated by the MCSM calculations, represented by the solid line in Fig. 5. In the MCSM approach,

TABLE II. Lifetime $\tau_{2_1^+}$ and transition probability $B(E2; 0^+_{g.s.} \rightarrow 2^+_1)$ for the 2^+_1 state in ^{112}Sn, compared with existing estimates.

$\tau_{2_1^+}$[a] (ps)	$\tau_{2_1^+}$[b] (ps)	$\tau_{2_1^+}$[c] (ps)	$\tau_{2_1^+}$[d] (ps)	$B(E2)$[a] (e^2b^2)	$B(E2)$[d] (e^2b^2)	$B(E2)$[e] (e^2b^2)	$B(E2)$[f] (e^2b^2)	$B(E2)$[g] (e^2b^2)	$B(E2)$[h] (e^2b^2)
$0.566^{+0.029}_{-0.038}$	$0.535^{+0.100}_{-0.080}$	0.800(110)	0.65(4)	$0.229^{-0.011}_{+0.016}$	0.199(11)	0.250(10)	0.242(11)	0.239(9)	0.242(23)

[a]Present measurement.
[b]^{112}Sn$(n, n'\gamma)$ [32].
[c]^{112}Sn$(p, p'\gamma)$ Spieker *et al.* [30].
[d]Jungclaus *et al.* [28].
[e]Allmond *et al.* [5].
[f]Kumar *et al.* [4].
[g](^{7}Li, ^{7}Li′) [11].
[h](^{12}C, ^{12}C′) [13].

the effective charges are taken as $1.25e$ and $0.75e$ for protons and neutrons, respectively. The model space consists of the $1g_{9/2,7/2}$, $2d_{5/2,3/2}$, $3s_{1/2}$, $1h_{11/2}$, $2f_{7/2}$, and $3p_{3/2}$ single-particle orbits for the neutrons as well as protons. Reference [26] reports further details about the MCSM calculations. The enhancement of quadrupole collectivity in ^{112}Sn can be primarily explained in terms of the strong proton excitation from the $1g_{9/2}$ orbit ($1g_{9/2} \rightarrow 2d_{5/2}$ being the most important), accompanied with the neutron deformation via enhanced proton-neutron interaction. Consequently, the contribution of core protons to the $E2$ transition matrix element for ^{112}Sn is found to be larger than 30%. The MCSM wave function is expressed as a superposition of the angular-momentum-projected Slater determinants, called basis vectors. In order to discuss the structure of the wave function before the projection, the intrinsic quadrupole moments of the unprojected basis vectors, Q_0 ($\propto \langle 2z^2 - x^2 - y^2 \rangle$) and Q_2 ($\propto \langle x^2 - y^2 \rangle$), are plotted on the potential energy surface obtained by the Q-constrained Hartree-Fock method [51], leading to a representation called the T plot. The x, y, and z coordinates taken in the intrinsic frame.

Figsures 6 and 7 show the T plots for the $0^+_{g.s.}$ and 2^+_1 states, respectively. The contour lines show the energy surface obtained by the Q-constrained Hartree-Fock method with the variation after parity projection. The locations of the circles indicate the intrinsic shape of the MCSM basis states, with the vertex defining the spherical limit. The size of each circle denotes the overlap probability of the MCSM basis state and the total wave function, viz., its importance in the total wave function. From Figs. 6 and 7, both the $0^+_{g.s.}$ and 2^+_1 states in ^{112}Sn are seen to have modest oblate deformations, thus leading to an enhanced $B(E2; 0^+_{g.s.} \rightarrow 2^+_1)$ value, as reported in Table II. The T plot shown in Fig. 6 clearly indicates absence of pairing correlations for the $0^+_{g.s.}$ state, leading to the nonspherical ground state in ^{112}Sn. This is consistent with the trend of MCSM calculations for the $^{100-110}$Sn isotopes [26], wherein the spherical ground state of the doubly closed ^{100}Sn isotope gives way to an increasingly prolate shape as the $1g_{7/2}$ orbit is filled up to ^{108}Sn. Thereafter, the neutrons occupying

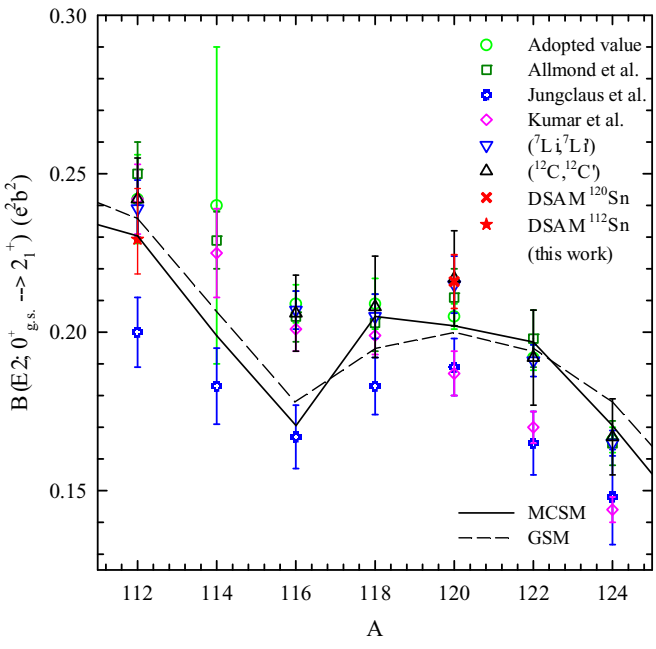

FIG. 5. Systematic plot of $B(E2; 0^+_{g.s.} \rightarrow 2^+_1)$ values for the stable even-mass Sn isotopes using the data obtained from several recent measurements [4,5,11,13,14,28,34], and the one from the present measurement for the ^{112}Sn isotope. The dashed and solid lines represent the GSM [23] and the MCSM [26] calculations, respectively.

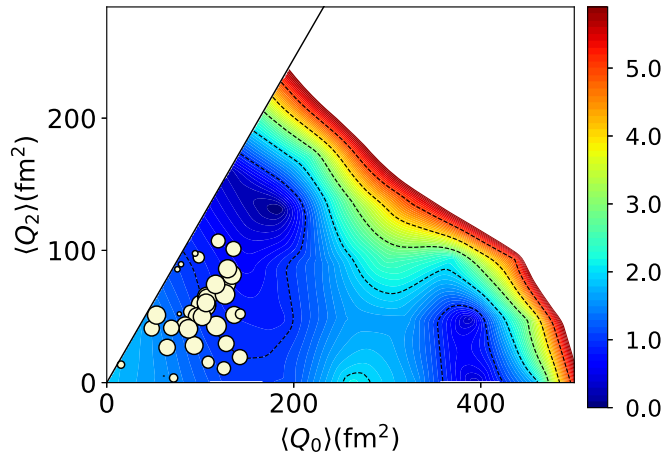

FIG. 6. T plot of the $0^+_{g.s.}$ state in ^{112}Sn coordinated by the intrinsic moments, Q_0 and Q_2.

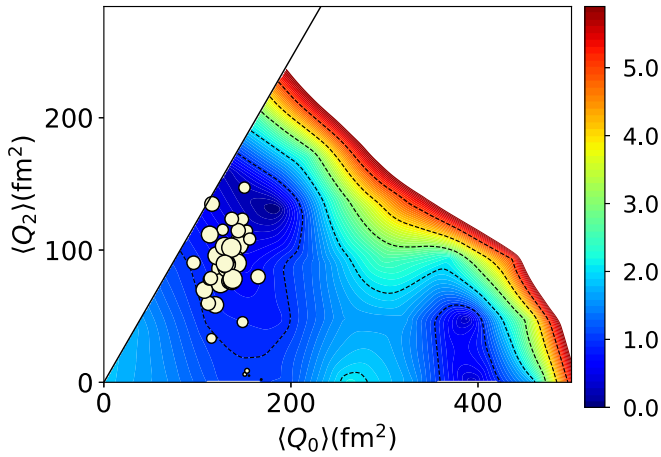

FIG. 7. T plot of the 2_1^+ state in ^{112}Sn coordinated by the intrinsic moments, Q_0 and Q_2.

the $2d_{5/2}$ orbit favor larger deformation for ^{110}Sn, with an oblate shape. As the $1g_{7/2}$-$2d_{5/2}$ neutron orbits become more than half-filled in ^{112}Sn, combined with the proton excitations from the the $1g_{9/2}$ orbit, the shape and deformation are expected to become saturated, with ^{110,112}Sn accounting for the highest $B(E2; 0^+_{\text{g.s.}} \rightarrow 2^+_1)$ values among the Sn isotopes. In this context, the present result is closely comparable to the measured $B(E2; 0^+_{\text{g.s.}} \rightarrow 2^+_1)$ values for the ^{110}Sn nucleus reported in Refs. [19,21].

IV. SUMMARY

The mean lifetime of the 2_1^+ level in ^{112}Sn has been determined using the Doppler-shift attenuation method implemented through updated methodologies, and an enhanced value of the corresponding transition probability is deduced therefrom. Existing measurements of the 2_1^+ lifetime have reported either a discrepant result on collective property or a value with larger uncertainty. The present $B(E2; 0^+_{\text{g.s.}} \rightarrow 2^+_1)$ value is in good agreement with those from recent measurements on Coulomb excitation, as well as $n-$, $\alpha-$, and heavy-ion scattering. Theoretical formalisms employing the generalized seniority model (GSM) scheme and contemporary Monte Carlo shell model (MCSM) calculations give a fairly good description of the experimental value. The enhancement is explained by the MCSM formalism in terms of oblate nature of the deformations for both the $0^+_{\text{g.s.}}$ and 2_1^+ states in ^{112}Sn, owing to strong proton-core excitations, accompanied by enhanced proton-neutron interactions.

In addition, an upper limit for the lifetime of the 3_1^- level is also presented, which is in compliance with the result from an extensive measurement of the low-lying structure in ^{112}Sn by the ^{112}Sn$(n, n'\gamma)$ reaction.

ACKNOWLEDGMENTS

The authors are grateful to the staff at the TIFR-BARC Pelletron Linac Facility for smooth operation of the accelerator during the experiment. This work is supported by the Department of Atomic Energy, Government of India (Project Identification Code 12-R&D-TFR-5.02-0200) and the Department of Science and Technology, Government of India (Grant No. IR/S2/PF-03/2003-II). H.P. is grateful for the support of the Ramanujan Fellowship Research Grant under SERB-DST (SB/S2/RJN-031/2016), Government of India. R.P., N.S., and E.I. acknowledge the RCNP Collaboration Research network (COREnet) program. E.I. acknowledges KAKENHI Grant No. 17H02893.

[1] P. H. Stelson, F. K. McGowan, R. L. Robinson, and W. T. Milner, Phys. Rev. C **2**, 2015 (1970).
[2] R. Graetzer, S. M. Cohick, and J. X. Saladin, Phys. Rev. C **12**, 1462 (1975).
[3] N. G. Jonsson, A. Backlin, J. Kantele, R. Julin, M. Luontarna, and A. Passoja, Nucl. Phys. A **371**, 333 (1981).
[4] R. Kumar, M. Saxena, P. Doornenbal, A. Jhingan, A. Banerjee, R. K. Bhowmik, S. Dutt, R. Garg, C. Joshi, V. Mishra *et al.*, Phys. Rev. C **96**, 054318 (2017).
[5] J. M. Allmond, A. E. Stuchbery, A. Galindo-Uribarri, E. Padilla-Rodal, D. C. Radford, J. C. Batchelder, C. R. Bingham, M. E. Howard, J. F. Liang, B. Manning *et al.*, Phys. Rev. C **92**, 041303(R) (2015).
[6] J. Bryssinck, L. Govor, V. Y. Ponomarev, F. Bauwens, O. Beck, D. Belic, P. von Brentano, D. DeFrenne, T. Eckert, C. Fransen *et al.*, Phys. Rev. C **61**, 024309 (2000).
[7] T. H. Curtis, R. A. Eisenstein, D. W. Madsen, and C. K. Bockelman, Phys. Rev. **184**, 1162 (1969).
[8] O. Beer, A. E. Behay, P. Lopato, Y. Terrien, G. Vallois, and K. K. Seth, Nucl. Phys. A **147**, 326 (1970).
[9] W. Makofske, W. Savin, H. Ogata, and T. H. Kruse, Phys. Rev. **174**, 1429 (1968).
[10] G. Bruge, J. C. Faivre, H. Faraggi, and A. Bussiere, Nucl. Phys. A **146**, 597 (1970).
[11] A. Kundu, S. Santra, A. Pal, D. Chattopadhyay, R. Tripathi, B. J. Roy, T. N. Nag, B. K. Nayak, A. Saxena, and S. Kailas, Phys. Rev. C **99**, 034609 (2019).
[12] L. R. Gasques, A. S. Freitas, L. C. Chamon, J. R. B. Oliveira, N. H. Medina, V. Scarduelli, E. S. Rossi, M. A. G. Alvarez, V. A. B. Zagatto, J. Lubian *et al.*, Phys. Rev. C **97**, 034629 (2018).
[13] A. Kundu, S. Santra, A. Pal, D. Chattopadhyay, T. N. Nag, R. Gandhi, P. C. Rout, B. J. Roy, B. K. Nayak, and S. Kailas, Phys. Rev. C **100**, 024614 (2019).
[14] S. Raman, C. Nestor, and P. Tikkanen, At. Data Nucl. Data Tables **78**, 1 (2001).
[15] I. O. Morales, P. V. Isacker, and I. Talmi, Phys. Lett. B **703**, 606 (2011).
[16] A. Banu, J. Gerl, C. Fahlander, M. Górska, H. Grawe, T. R. Saito, H.-J. Wollersheim, E. Caurier, T. Engeland, A. Gniady *et al.*, Phys. Rev. C **72**, 061305(R) (2005).
[17] D. Radford, C. Baktash, J. Beene, B. Fuentes, A. Galindo-Uribarri, J. G. del Campo, C. Gross, M. Halbert, Y. Larochelle, T. Lewis *et al.*, Nucl. Phys. A **746**, 83c (2004).

[18] P. Doornenbal, P. Reiter, H. Grawe, H. J. Wollersheim, P. Bednarczyk, L. Caceres, J. Cederkäll, A. Ekström, J. Gerl, M. Górska *et al.*, Phys. Rev. C **78**, 031303(R) (2008).
[19] C. Vaman, C. Andreoiu, D. Bazin, A. Becerril, B. A. Brown, C. M. Campbell, A. Chester, J. M. Cook, D. C. Dinca, A. Gade *et al.*, Phys. Rev. Lett. **99**, 162501 (2007).
[20] P. Doornenbal, S. Takeuchi, N. Aoi, M. Matsushita, A. Obertelli, D. Steppenbeck, H. Wang, L. Audirac, H. Baba, P. Bednarczyk *et al.*, Phys. Rev. C **90**, 061302(R) (2014).
[21] J. Cederkäll, A. Ekström, C. Fahlander, A. M. Hurst, M. Hjorth-Jensen, F. Ames, A. Banu, P. A. Butler, T. Davinson, U. DattaPramanik *et al.*, Phys. Rev. Lett. **98**, 172501 (2007).
[22] A. Ansari, Phys. Lett. B **623**, 37 (2005).
[23] B. Maheshwari, A. K. Jain, and B. Singh, Nucl. Phys. A **952**, 62 (2016).
[24] N. Shimizu, T. Abe, M. Honma, T. Otsuka, T. Togashi, Y. Tsunoda, Y. Utsuno, and T. Yoshida, Phys. Scr. **92**, 063001 (2017).
[25] T. Otsuka, M. Honma, T. Mizusaki, N. Shimizu, and Y. Utsuno, Prog. Part. Nucl. Phys. **47**, 319 (2001).
[26] T. Togashi, Y. Tsunoda, T. Otsuka, N. Shimizu, and M. Honma, Phys. Rev. Lett. **121**, 062501 (2018).
[27] S. Devons, G. Manning, and D. S. P. Bunbury, Proc. Phys. Soc. A **68**, 18 (1955).
[28] A. Jungclaus, J. Walker, J. Leske, K.-H. Speidel, A. Stuchbery, M. East, P. Boutachkov, J. Cederkäll, P. Doornenbal, J. Egido *et al.*, Phys. Lett. B **695**, 110 (2011).
[29] M. East, A. Stuchbery, A. Wilson, P. Davidson, T. Kibédi, and A. Levon, Phys. Lett. B **665**, 147 (2008).
[30] M. Spieker, P. Petkov, E. Litvinova, C. Müller-Gatermann, S. G. Pickstone, S. Prill, P. Scholz, and A. Zilges, Phys. Rev. C **97**, 054319 (2018).
[31] A. Kumar, J. N. Orce, S. R. Lesher, C. J. McKay, M. T. McEllistrem, and S. W. Yates, Phys. Rev. C **72**, 034313 (2005).
[32] J. N. Orce, S. N. Choudry, B. Crider, E. Elhami, S. Mukhopadhyay, M. Scheck, M. T. McEllistrem, and S. W. Yates, Phys. Rev. C **76**, 021302(R) (2007).
[33] J. N. Orce, S. N. Choudry, B. Crider, E. Elhami, S. Mukhopadhyay, M. Scheck, M. T. McEllistrem, and S. W. Yates, Phys. Rev. C **77**, 029902(E) (2008).
[34] A. Kundu, S. Santra, A. Pal, D. Chattopadhyay, R. Raut, R. Palit, M. S. R. Laskar, F. S. Babra, C. S. Palshetkar, B. K. Nayak *et al.*, Phys. Rev. C **100**, 034327 (2019).
[35] H. Pai, S. Ali, S. Rajbanshi, P. Ray, S. Roy, and A. Goswami, Vacuum **167**, 393 (2019).
[36] R. Palit, S. Saha, J. Sethi, T. Trivedi, B. S. Naidu, P. B. Chavan, R. Donthi, and S. Jadhav, J. Phys.: Conf. Ser. **420**, 012159 (2013).
[37] S. Ganguly, P. Banerjee, I. Ray, R. Kshetri, R. Raut, S. Bhattacharya, M. Saha-Sarkar, A. Goswami, S. Mukhopadhyay, A. Mukherjee *et al.*, Nucl. Phys. A **789**, 1 (2007).
[38] R. Palit, S. Saha, J. Sethi, T. Trivedi, S. Sharma, B. Naidu, S. Jadhav, R. Donthi, P. Chavan, H. Tan *et al.*, Nucl. Instrum. Methods Phys. Res. A **680**, 90 (2012).
[39] S. Das, S. Samanta, R. Bhattacharjee, R. Raut, S. Ghugre, A. Sinha, U. Garg, R. Chakrabarti, S. Mukhopadhyay, A. Dhal *et al.*, Nucl. Instrum. Methods Phys. Res. A **841**, 17 (2017).
[40] J. C. Wells and N. R. Johnson, Report No. ORNL-6689, 44 (1991).
[41] S. Lalkovski and F. Kondev, Nucl. Data Sheets **124**, 157 (2015).
[42] I. J. Thompson and F. M. Nunes, *Nuclear Reactions for Astrophysics* (Cambridge University Press, New York, 2009).
[43] P. David, J. Bisplinghoff, M. Blann, T. Mayer-Kuckuk, and A. Mignerey, Nucl. Phys. A **287**, 179 (1977).
[44] J. Lindhard, M. Scharff, and H. E. Schiott, Mat. Fys. Medd. Dan. Vid. Selsk. **33**, 1 (1963).
[45] J. Ziegler, *The Stopping and Ranges of Ions in Matter* (Pergamon, Oxford, 1980), Vol. 3.
[46] L. Northcliffe and R. Schilling, At. Data Nucl. Data Tables **7**, 233 (1970).
[47] H. Paul and A. Schinner, Nucl. Instrum. Methods Phys. Res., Sect. B **209**, 252 (2003).
[48] http://www.srim.org.
[49] R. Bhattacharjee, S. S. Bhattacharjee, K. Basu, P. V. Rajesh, R. Raut, S. S. Ghugre, D. Das, A. K. Sinha, L. Chaturvedi, U. Garg *et al.*, Phys. Rev. C **90**, 044319 (2014).
[50] A. Gavron, Phys. Rev. C **21**, 230 (1980).
[51] T. Otsuka and Y. Tsunoda, J. Phys. G: Nucl. Part. Phys. **43**, 024009 (2016).